CLAS-Note 96-022

CLAS Region I Prototype Detector

Daniel S. Carman
Department of Physics
Carnegie Mellon University
carman@ernest.phys.cmu.edu

November 26, 1996

1 Introduction

The Region I prototype sector consists of six individual drift cells in the axial (or inner) superlayer positioned along the extent of the endplates at representative locations to span nearly the full polar angular range subtended by the Region I detector. The prototype detector also contains one fully instrumented section outfitted with a single signal translator board (STB) and high voltage translator board (HVTB). This portion of the detector was originally constructed to enable tracking studies with cosmic rays through a more realistic Region I sector geometry. This instrumented portion of the sector consists of roughly 64 drift cells in the stereo (or outer) superlayer and roughly 96 drift cells in the axial supterlayer. Note that this prototype sector has opposite orientations of the axial and stereo superlayers relative to the final Region I sectors.

The positions of each of these active areas of the prototype have been crudely measured with respect to the nominal CLAS solid target location. The drift cells have been labelled consecutively from sector nose to sector tail as P1 though P6, respectively. The positions are included in the following table, where Θ_{CLAS} represents the measured polar angle.

Cell	Θ_{CLAS}
P1	13°
P2	22°
P3	35°
P4	55°
P5	75°
P6	140°
I.S.	$85^\circ \rightarrow 129^\circ$

The angle measurements for the individual drift cells were made from the nominal CLAS solid target position to the sense wire. The measurements for the instrumented section were made from the target position to the upstream and downstream 'end walls' of this section of the sector.

The nominal layout for each of the individual drift cells is shown in Fig. 1. The diameter of the gas bags at the endplates is 2.75 in for cells P1 $\rightarrow$ P3, and 3.25 in for cells P4 $\rightarrow$ P6. The gas bag was constructed from aluminized coated nylon with the conductive surface on the inside of the cell. This aluminized coating is not electrically connected to a region of defined potential. The individual drift cells consist of six guard wires and six field wires strung with 140 μm diameter gold-plated aluminum wires, and one sense wire strung with 20 μm diameter gold-plated tungsten wire. The distance from the sense wire to each field wire is 8 mm, and the distance from the sense wire to each guard wire is 14mm. Note that Fig. 1 only represents and idealized cell layout. In some cases, due to existing structures on the endplates of the prototype, the wires of the cell were not centered within the gas volume.

The high voltage and readout configuration for each of the individual drift cells is shown

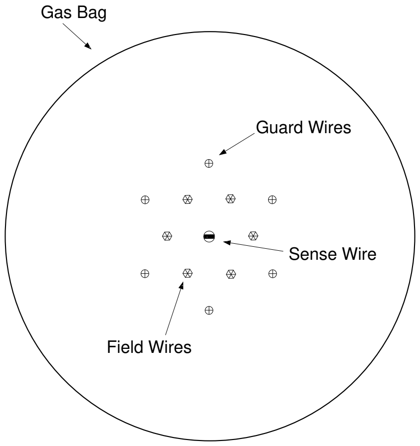

Figure 1: Schematic representation of one of the individual drift cells of the prototype. Figure is drawn roughly to scale.

in Fig. 2. These drift cells were designed to employ negative high voltage on the guard and field wires while keeping the sense wire at ground potential. The left half of Fig. 2 shows the low pass filter added to the guard and field wires to help reduce pickup of high frequency noise components. Note that all six guard wires in each cell and all six field wires in each cell are bussed together using wire wrap on the crimp pins. The right half of Fig. 2 shows the sense wire connected to ground through a 1 MΩ resistor on one side of the wire, and connected to the STB on the instrumented section of the chamber on the other side of the wire. The sense wires of the individual cells have been configured to be readout through channels on the STB of the instrumented section by removing conductive rubber booties on the STB and sacrificing six drift cells of this instrumented portion of the chamber. The sense wires of the individual drift cells are connected to the STB through coaxial lines strung along the endplate.

Our studies of the individual drift cells clearly show that the current drawn on the sense wire is equal in magnitude and opposite in sign to the sum of the currents drawn on the six field wires. As well, studies of the output from the GARFIELD potential/field line program with our cell geometry dictate that the best operating point for the drift cells is a setting where $V_{field} = 2V_{guard}$. A representative calculation of the electric field configuration for one of our drift cells at its nominal plateau voltage settings in a 50%-50% argon/ethane gas mixture is shown in Fig. 3.

2 Efficiency Measurements

Efficiency measurements have been performed on the prototype sector with two different gas mixtures. These two mixtures are argon/ethane (62% - 38% molar) and argon/CO_2 (85% - 15% molar). The argon/ethane gas mixture, which will be employed for data acqui-

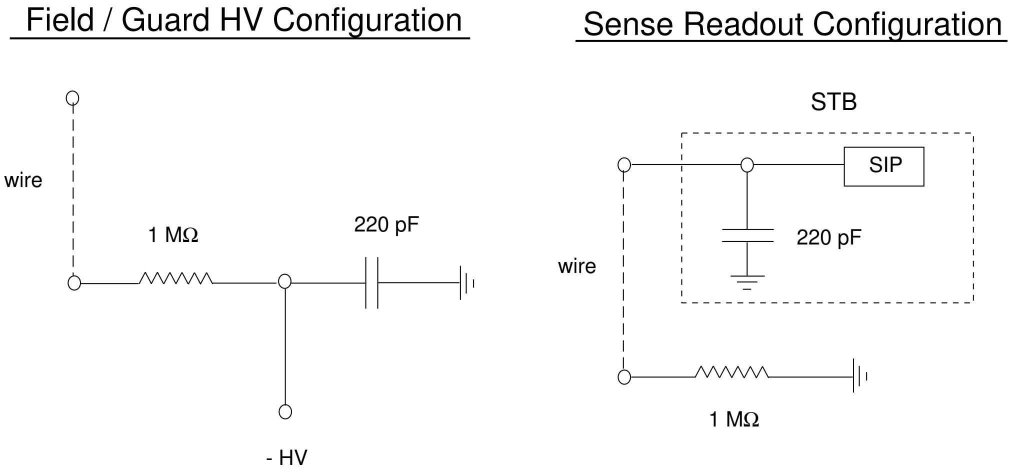

Figure 2: Schematic representation of the HV configuration for the guard and field busses of the individual drift cells (left) and the readout configuration of the sense wires of the individual drift cells (right).

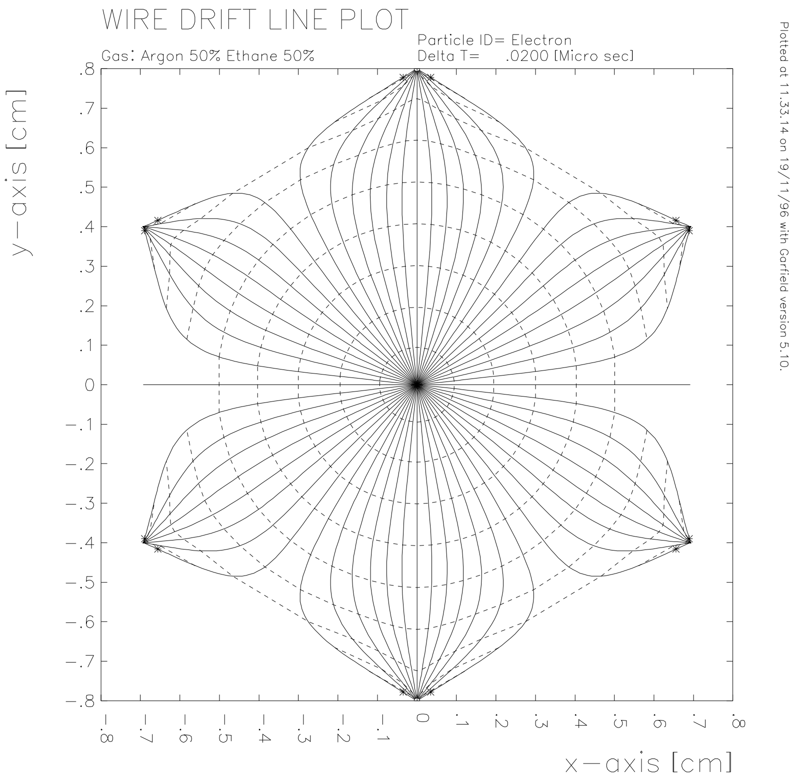

Figure 3: Results of a GARFIELD field line calculation of a single prototype drift cell in a 50-50 argon/Ethane environment with V_{field} =-2400 V, V_{guard} = -1200 V, and V_{sense} = 0 V.

sition with the final Region I detector, has been studied in some detail at the University of Pittsburgh. These measurements show that the appropriate operating point for the Region I detector (i.e. just above the knee in the plateau curve) is V_{sense} = 1200 V, V_{field} = -1200 V, V_{guard} = +300 V. Efficiency measurements using argon/CO_2, which will be employed in the prototype for the December 1996 beam time, have been performed for both the instrumented section and for an individual drift cell (P5). Both measurements employed a pair of plastic scintillators (S1,S2) above and below the detector to define cosmic rays passing through the drift cell. The efficiency definition for both measurements was defined to be:

$$\epsilon = \frac{S1 \cdot S2 \cdot \mathrm{wire}}{S1 \cdot S2}. \tag{1}$$

The detector layout and electronics configuration for the efficiency measurements of drift cell P5 are shown in Fig. 4. The top half of this figure shows the placement and dimensions of the scintillators. The bottom half of this figure shows the electronics set up employed for the measurement. In this figure there are two visual scalers used to count S1·S2·wire (≡NUM) and S1·S2 (≡DEN). Note that the gate and delay generator on the wire output was employed to prevent double-pulsing of the wire signal. This hold-off was not employed for the efficiency measurements on the instrumented section of the prototype.

As was mentioned earlier, the individual drift cells are read out through the STB on the instrumented section. The SIP output (with a gain of 2.2 mV/μA) was fed to a VPI postamplifier (with a gain of 10) before being sent to a leading edge discriminator. For cell P5, this discriminator was set just above the noise at a threshold of -20 mV. For the instrumented section of the prototype the noise pickup immunity is much better than for the individual drift cells. This allowed efficiency measurements to be made at both -10 mV and -20 mV discriminator thresholds.

Fig. 5 shows the efficiency result for drift cell P5 for the argon/CO_2 gas mixture. The efficiency is plotted as a function of the field voltage. During this measurement, the guard voltage was set to one half of the field voltage, and the sense wire was held at ground. The measurement shows a knee at around -2250 V. Above -2600 V the cell discharge due to streamers begins to dominate the signal. The error bars shown represent the statistical error of the measurement. The efficiency of cell P5 is seen to reach a maximum of $\epsilon_{max} \approx 35\%$. This value makes reasonable sense given the detector and cell geometries. Consider the ratio of the drift cell diameter to the width of scintillator S2. This ratio should provide a good estimate of the maximum obtainable efficiency.

$$R = \frac{16\ mm}{52\ mm} = 32\% \tag{2}$$

Fig. 6 shows the efficiency measurement for the instrumented section of the Region I prototype for the argon/CO_2 gas mixture. The efficiency is plotted as a function of the difference between the sense and field voltages for a fixed field voltage of -1100 V. In all cases the guard wires were held at ground potential. The two measurements shown are for the two discriminator thresholds employed, -10 mV and -20 mV.

It is clear from this figure that the efficiency curves for the instrumented section are not as smoothly varying as those for cell P5, especially for the lower threshold setting. This is

Detector layout for efficiency measurement:

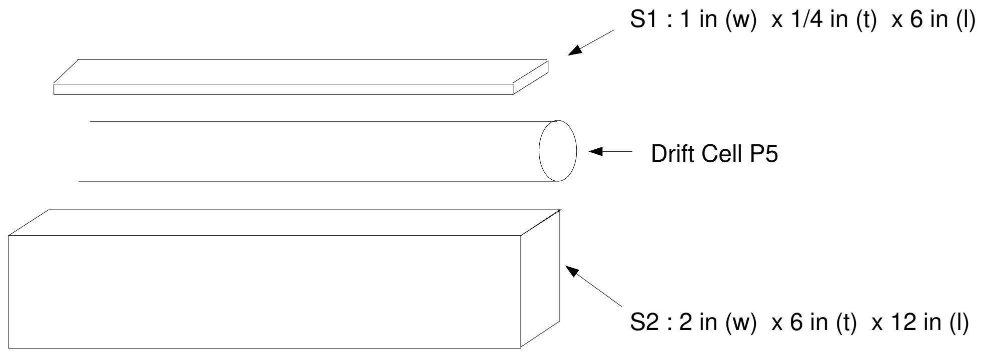

Electronics layout for efficiency measurement:

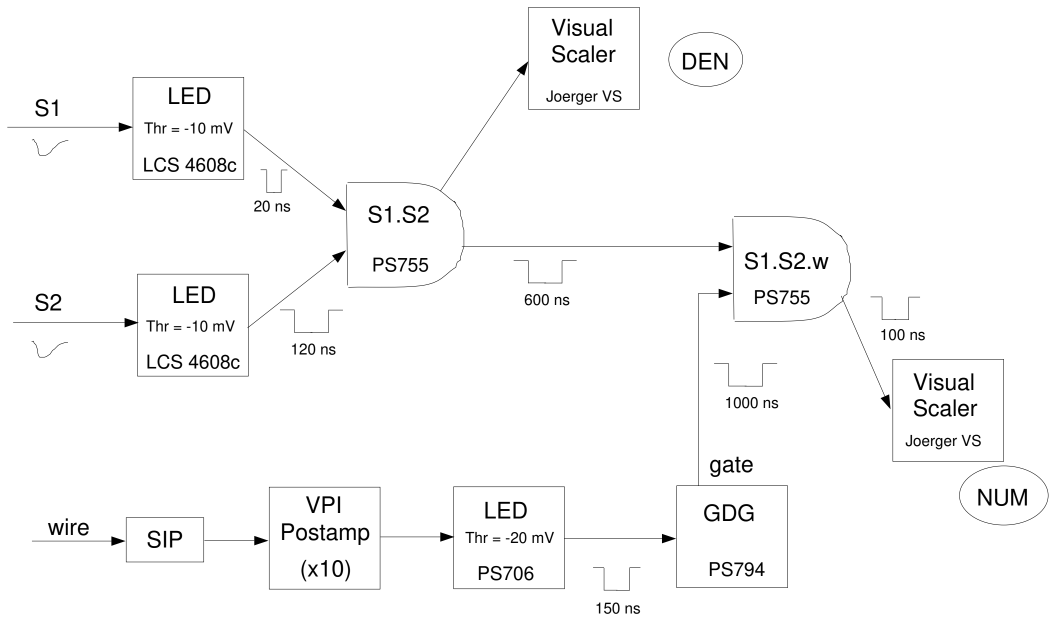

Figure 4: The top half of this figure shows the detector layout for the efficiency measurement of drift cell P5. The bottom half of this figure shows the electronics scheme for the measurement.

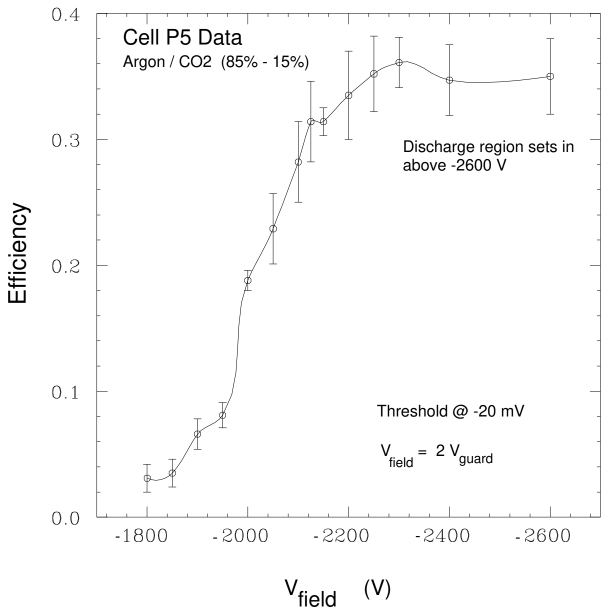

Figure 5: Cell P5 efficiency measured as a function of the field voltage in an argon/CO_2 (85% - 15% molar) environment at a threshold of -20 mV.

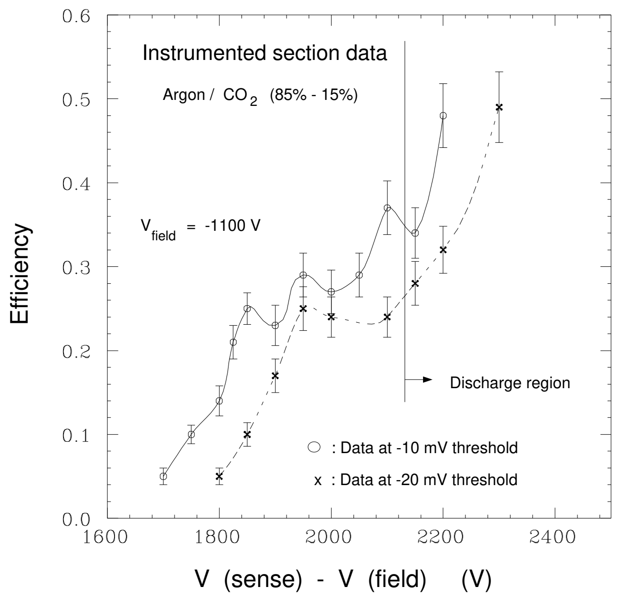

Figure 6: Instrumented section efficiency measured as a function of the difference between the sense and field voltages in an argon/CO_2 environment at thresholds of -10 mV and -20 mV.

most likely due to the fact that -10 mV was just at the level of the high frequency pickup noise. However we see a knee in the plateau curve round -1950 V. Above about -2150 V discharge begins to dominate the signal. Again, the error bars shown represent the statistical uncertainty of the measurement.

The voltage axes in Fig. 5 for cell P5 and Fig. 6 for the instrumented section have been chosen to allow for direct comparison of the two measurements. For cell P5 the knee in the efficiency occurs at $\sim$ -2250 V, whereas for the instrumented section it occurs roughly 300 V lower. There are two possible explanations for these differences. The first is that the isolated drift cells have less efficiency far from the sense wire due to the lack of neighboring cells. This could result in a lower electric field between the field wires, and hence less efficiency. Our GARFIELD calculations comparing the two cases indicate that this argument may have validity at some level. The other explanation could be attributed to differences in capacitance between the isolated drift cells and the cells of the instrumented section. The difference in capacitance results as the sense wires of the isolated drift cells are connected to the STB through lengths of coaxial cable, whereas the sense wires of the instrumented section are connected directly to the STB in the usual fashion.

3 Gain Measurements

Measurements of the prototype gas gain have been performed for each of the individual drift cells employing both argon/ethane (62%-38% molar) and argon/CO_2 (85%-15% molar). These measurements employed an ^{55}Fe source which produces 5.9 keV gamma rays.

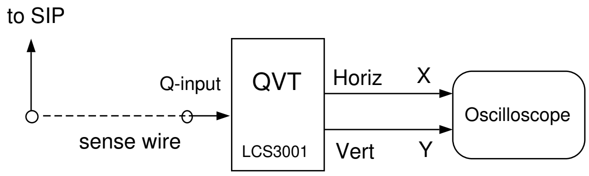

Figure 7: Electronics configuration for the drift cell gain measurements.

As shown in Fig. 7, the output of the sense wire was taken directly into the Q-input of a QVT (no amplification through a SIP or a postamplifier). The horizontal and vertical outputs of the QVT were connected to a fast oscilloscope operated in X-Y mode. The oscilloscope then shows a two dimensional representation of the number of counts versus charge collected. The QVT was gated internally with a gate width set to 200 nsec. The QVT threshold was set to reduce the noise at levels ranging from -1 mV (at the lowest gains) to -10 mV (at the highest gains). Given the measured channel of the peak of the 5.9 keV gamma rays in the QVT charge spectrum along with the conversion gain of the QVT, the gas gain can be determined as:

$$G = \frac{(QVT \text{ channel}) \cdot G_{QVT}}{Q_e \cdot N_{Fe}}. \qquad (3)$$

In this equation, G_{QVT} represents the selected conversion gain of the QVT (1 pC/channel), Q_e represents the electron charge (1.602×10^{-19} coul/electron), and N_{Fe} represents the number of electrons liberated from the 5.9 keV gamma ray (228). The value of N_{Fe} is actually only strictly valid in a gas mixture of argon/ethane (50% - 50%), but is a reasonable approximation for the two gas mixtures under study here.

Fig. 8 shows the measured gain plotted against the field voltage for the individual drift cells operated in both argon/ethane and argon/CO_2 environments. As the gains for each of the drift cells P1 $\rightarrow$ P6 were quite similar, the curves in Fig. 8 represent an average over the six cells. For these measurements the guard voltage was set to one half the field voltage, and the sense wire was held at ground. The gains are seen to vary between 10^5 and 10^6 over the range of voltages studied. Keep in mind that the field voltages at which the gain measurements were made were necessarily at the high end of the values employed for the efficiency measurements due to the fact that no amplification was used for the gain measurements. This lack of amplification was felt necessary to remove the uncertainty in the current-dependent gain of the SIP's on the STB. This then provides for a more direct measurement of the gas gain.

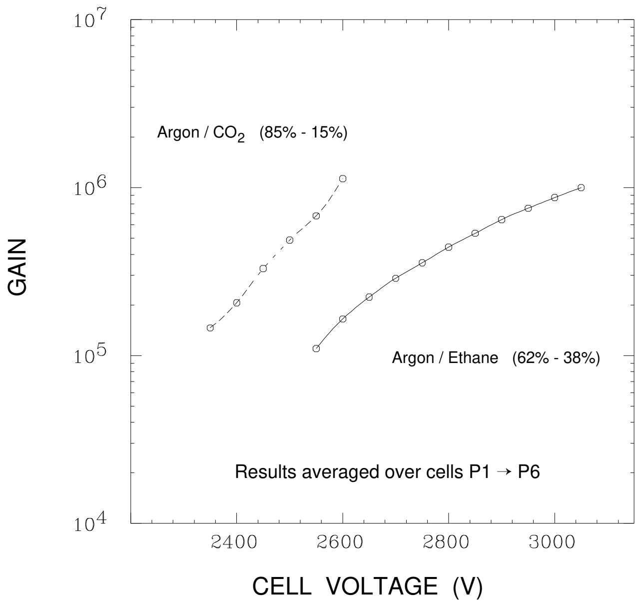

Figure 8: Measured gain averaged over the six individual drift cells plotted as a function of the magnitude of the field voltage. Measurements are shown for both argon/ethane (62% - 38% molar) and argon/CO_2 (85% - 15% molar).

The gas gain measurements for the prototype cells in the argon/ethane (62% - 38% molar) environment can be compared to the results of the SKELETON gas gain calculation by M. Mestayer [1]. The gas gain is calculated to be:

$$G = 2^{N_d}, \qquad N_d = \frac{R_{crit} - R_w}{\mathrm{mfp_h}}. \tag{4}$$

In this expression, R_{crit} represents the distance that the avalanche begins from the sense wire, R_w is the radius of the sense wire, and mfp_h represents the mean free path over which the ionization avalanche doubles. Therefore the exponent N_d represents the number of doubling lengths. R_{crit} can be expressed further as:

$$R_{crit} = \frac{V_{field}}{E_{crit} - log(D/R_w)} \qquad = \qquad \frac{V_{field} - \mathrm{mfp_l}}{PE_{Ar} - log(D/R_w)}. \tag{5}$$

In this expression, V_{field} represents the field voltage of the drift cell, E_{crit} represents the electric field strength at which the ionization avalanche begins, PE_{Ar} represents the ionization potential energy for argon, D represents the maximum drift distance, and mfp_l represents the mean free path at unity gain. The two different mean free paths used to calculate the gas gain were determined from a two parameter fit (slope, intercept) to plots of normalized current versus voltage for a straw tube illuminated by a UV light source.

Fig. 9 shows a comparison of our prototype gas gain measurements in an argon/ethane (62% - 38% molar) environment to the SKELETON results for an argon/ethane (50% - 50%) gas mixture. The results of the calculation differ from our measurements in two respects, namely there is a clear difference in the slope of the gain curves, as well as a difference in the calculated versus measured gains. The changing slope of the prototype cell data may result from a saturation effect due to space charge build-up around the sense wire as the gain increases. At the lower voltages it appears that there is a reasonable agreement between the slopes of the data and the calculation.

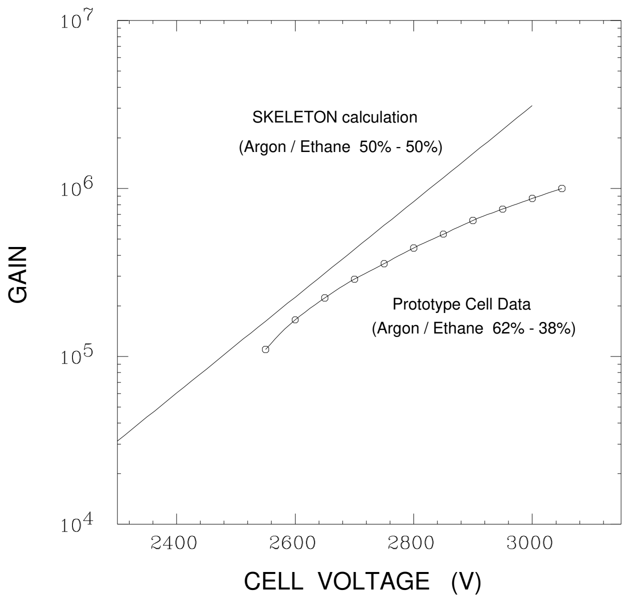

Figure 9: Measured gain averaged over the six individual drift cells plotted as a function of the magnitude of the field voltage for argon/ethane (62% - 38% molar) compared with the results of the SKELETON gas gain calculation assuming an argon/ethane mixture (50% -50%).

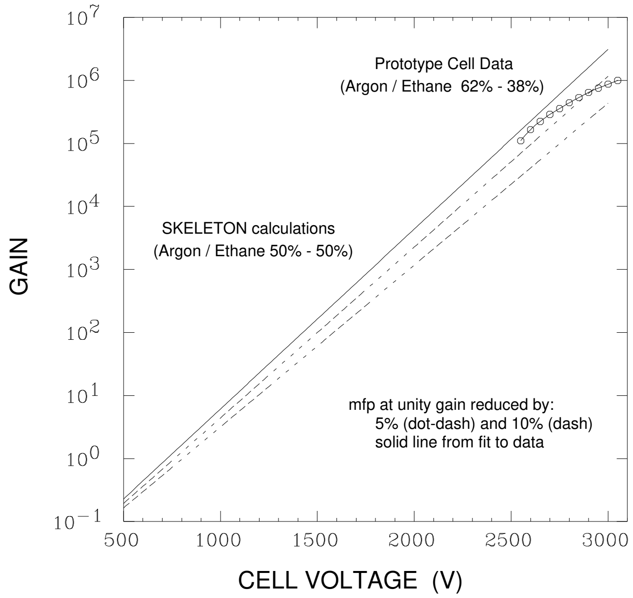

Figure 10: Measured gain averaged over the six individual drift cells plotted as a function of the magnitude of the field voltage for argon/ethane (62% - 38% molar) compared with the results of the SKELETON gas gain calculation assuming an argon/ethane (50% -50%) mixture. The mean free path at unity gain was varied in the different calculations by -5% and -10% relative to the fit value.

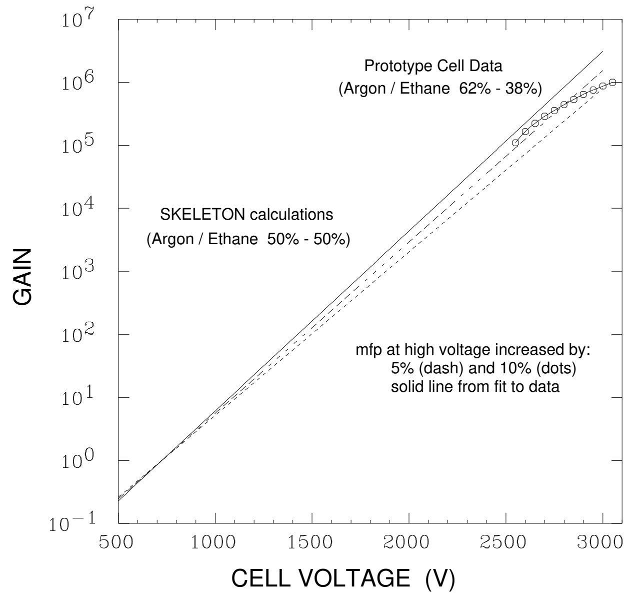

Figure 11: Measured gain averaged over the six individual drift cells plotted as a function of the magnitude of the field voltage for argon/ethane (62% - 38% molar) compared with the results of the SKELETON gas gain calculation assuming an argon/ethane (50% -50%) mixture. The mean free path at high voltages was varied in the different calculations by 5% and 10% relative to the fit value.

In an attempt to understand how uncertainties in the fit mean free paths affect the calculated gas gains, I have allowed them to vary by ±5% and ±10% as shown in Fig. 10 and Fig. 11. Fig. 10 shows that reducing the mean free path at unity gain (mfp_l) by ~5% brings the calculated gas gain much more into agreement with our measurements. Fig. 11 shows that increasing the mean free path at high voltages (mfp_h) by ~5% also brings the calculated gas gain much more into agreement with our measurements. These sorts of games clearly show that the calculations can provide for a reasonable representation (i.e. better than an order of magnitude) of the true gas gains.

4 Prototype Noise Measurements

After installation of the prototype detector into the CLAS cryostat, measurements were made of the required thresholds for the discriminators for cells P1 → P6 and the instrumented section. The measurements were made using a high frequence oscilloscope looking at the output of the sense wire after the SIP in the STB and a VPI postamplifier. The DC offset after the postamp was measured to be zero for all channels. The noise level (and hence the required discriminator threshold) is defined to be the oscilloscope threshold necessary such that less than 10% of the triggers are noise (characterized by pulse shape). The noise levels were measured at the prototype (as opposed to at the electronics rack) with the individual drift cells and the instrumented section set at their nominal plateau voltages (P1 → P6: V_{field} = -2200 V, V_{guard} = -1100 V, V_{sense} = 0 V, I.S.: V_{field} = -1100 V, V_{guard} = 0 V, V_{sense} = 900 V). The measured noise levels were as follows:

Cell	Noise amplitude (p-p)	I.S. Wire	Noise amplitude (p-p)
P1	300 mV	L5-1	24 mV
P2	230 mV	L5-2	20 mV
P3	190 mV	L5-3	28 mV
P4	170 mV	L5-4	28 mV
P5	120 mV	L5-5	24 mV
P6	40 mV	L5-6	24 mV

In studying the results of the noise measurements for the individual drift cells, we see a monotonically increasing level as we go from cell P6 in the sector tail to cell P1 in the sector nose. These results are consistent with my studies of the noise levels in the prototype in the EEL building in October 1996. This monotonic increase is directly correlated with the increase in length of the coaxial lines used to connect the sense wires of the individual cells to the STB. The results of my studies showed that the longer this coaxial line, the greater the noise amplitude. Keep in mind that as these noise measurements represent the peak-to-peak amplitude of the noise, the required discriminator thresholds will be a factor of two less.

For the individual drift cells several things were done to help reduce the pickup noise frequency and amplitude. For example, the addition of low pass filters on the field and guard high voltage busses reduced the noise frequency by an order of magnitude. As well, several different grounding schemes of the chamber, signal, and high voltage lines were studied. The best overall configuration seemed to be to let the ground braids on the signal coaxial lines and the SHV cables float. Also we verified that the noise was substantially reduced for the individual drift cells when the endplates were left floating and the electronics ground defined the chamber ground. Again we were pleased to see that the instrumented section was much less sensitive to these issues.

We still expect that even with the large discriminator thresholds required to suppress the noise levels that read out of these individual cells will provide us with useful information regarding the true raw rates of charged particles through the detector during the December beam time. After obtaining a spectrum of events from a 'quiet' cell such as P6, we can determine the raw rates in the other drift cells by scaling the measured rates based on the integrated spectrum of cell P6. Crudely speaking one could assume that the measured rates in each drift cell are related to the true rates in each drift cell by a scaling factor.

$$S_F = \frac{\int_{E_{Pn}}^{\infty} \text{(P6 spectrum)}}{\int_{E_{P6}}^{\infty} \text{(P6 spectrum)}} \tag{6}$$

In this expression the energy spectrum of cell P6 is integrated over energy limits defined by the threshold employed for cell Pn ($n = 1 \rightarrow 5$) in the numerator, and the threshold employed for cell P6 in the denominator.

By studying the noise levels in the much more noise immune instrumented section of the prototype, we see very uniform and low levels. This is very good news from the standpoint of the final Region I detector. Our goal is to set the chamber thresholds, and hence the chamber voltages, as low as possible while still maintaining high efficiencies. The lower the operating voltages can be set, the longer the chambers will survive within the intense raditation environment of CLAS.

5 Goals of the December Test Run

The prototype Region I detector has been installed into the CLAS spectrometer in the 5 o'clock position. The goals during this upcoming beam time in December, while rather a short list, are nevertheless extremely important to determine the range of beam-target luminosities that can be employed for the Hall B physics program. Basically, the limiting luminosity for the Region I detector will be the limiting luminosity for CLAS. The prototype sector has been designed and constructed primarily to address this issue. During the beam time we will be measuring the leakage currents in the prototype sector (drift cells P1 $\rightarrow$ P6 and the instrumented section) as a function of beam current and targt thickness. The other important parameter to correlate the detector leakage current with is the current in the minitoroid which is positioned just inside of Region I. This sizeable normal-conducting toroidal magnet was designed to limit the ionization entering the active portion of the Region I detectors by sweeping the low energy Moller electrons back towards the beam pipe. The individual drift cells in the Region I prototype were positioned to allow us to study the currents and rates as a function of polar scattering angle. These studies should help to determine the appropriate mini-torus magnetic field and the allowable CLAS luminosities.

A secondary goal of the upcoming test run is to attempt tracking of charged particles from the CLAS target through the instrumented portion of the prototype and the 5 o'clock Region II and Region III sectors. Analysis of this data as a function of momentum of the outgoing particles should allow a much more realistic tuneup of the CLAS tracking software. The only difficulty in this process is the lack of precise knowledge of the positions of the prototype sense wires relative to the CLAS coordinate system. However the positions should be known well enough to enable tracking studies in a realistic chamber background environment.

References

[1] M. Mestayer, Calculation of Drift Chamber Gas Gain, CLAS-Note 96-005.